AN EXPERIMENTAL AND NUMERICAL INVESTIGATION OF THE INTERACTION BETWEEN SPLITS AND EDGE DELAMINATIONS IN $[+20_m/-20_m]_{ns}$ CARBON/EPOXY LAMINATES

X. Xu[1*], M. R. Wisnom[1]

[1] *Advanced Composites Centre for Innovation & Science (ACCIS), University of Bristol, University Walk, Bristol BS8 1TR, UK*
**xiaodong.xu@bristol.ac.uk*

Keywords: angle ply, edge delamination, finite element analysis (FEA), interface element

Abstract
Experimental and numerical investigations were carried out to study ply thickness scaling effects of angle ply laminates and interaction between splits and edge delaminations. Two series of $[+20_m/-20_m]_{ns}$ laminates which are dispersed ply laminates ($m=1$, $n=8$) and blocked ply laminates ($m=2$, $n=4$) were tested under uniaxial tensile load. Additionally, interrupted tests were carried out to investigate the failure initiation mechanism. A FE method using the explicit code LS-Dyna with splitting and interface elements was applied to understand the failure process. Moreover, a simplified method was also used to predict the stress for the angle ply edge delamination initiation.

1 Introduction

Splits and delaminations initiating from the free edges are very important mechanisms in the failure of composite laminates. A number of studies have considered the failure mechanism of angle ply laminates. O'Brien[1] showed that free edges cause failure initiation due to high inter-laminar shear and normal stresses which can drive edge delaminations. Johnson and Chang[2] studied failure mechanism of different angle ply laminates. They divided edge delaminations into two types: angle ply edge delamination and mode I edge delamination. Studies of matrix induced angle ply edge delamination have been reported by O'Brien and Hooper[3,4], Yang and He[5], Lavoie and Morton[6], Johnson and Chang[2,7], Kashtalyan and Soutis[8-10] and Kobayashi et al.[11]. Ply thickness can also affect angle ply edge delamination. Thickness scaled angle ply laminates have been studied by Kellas and Morton[12], Lavoie and Morton[6], Johnson and Chang[2]. However, failure theories based on classical laminate theory (CLT) do not work because they consider neither inter-laminar stresses nor ply thickness scaling effects.

In this paper, to study ply thickness scaling effects of angle ply laminates, two series of $[+20_m/-20_m]_{ns}$ laminates which are the dispersed ply laminates (m=1, n=8) and the blocked ply laminates (m=2, n=4) were tested under uniaxial tensile load. In addition, interrupted tests were also carried out to see the failure initiation mechanism. Meanwhile, a FE method using the explicit code LS-Dyna with splitting and interface elements was applied to understand the failure process.

Unlike previous studies, the interaction between splits and angle ply edge delamination was considered, using predefined multiple potential splitting paths, so that the process of splitting and angle ply edge delamination initiation and propagation could be simulated. Finally, a simplified method based on O'Brien's approach[13] was also used to predict the stress for the angle ply edge delamination initiation.

2 Experimental setup

The specimen dimensions are shown in Figure 1.

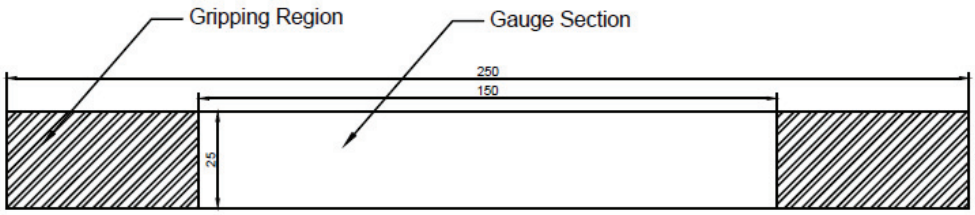

Figure 1. Specimen dimensions

The material used in this test was the IM7/8552 carbon-epoxy pre-preg with a nominal ply thickness of 0.125 mm. Two series of 32-ply specimens were used in the tests. Five 4mm-thick specimens were the dispersed ply laminates with $[+20/-20]_{8s}$ lay-up. The other five 4mm-thick specimens were the blocked ply laminates with $[(+20)_2/(-20)_2]_{4s}$ lay-up in which two adjacent plies with the same fibre orientation were blocked together to form 0.25mm-thick blocked plies. Tests were carried out on an Instron hydraulic-driven 250kN test machine under displacement control at a rate of 1mm/minute. Interrupted tests stopping at 90% of the failure load for each lay-up were carried out to capture the damage progress.

3 Finite element analysis (FEA)

In the FEA, material properties were the same for all cases. Cohesive zone interface elements were used to simulate matrix cracks within plies and delaminations between plies. The properties of the cohesive zone interface elements are shown in Table 1. The lamina properties are shown in Table 2. These properties were used in the FEA and assessments based on the conventional failure theories.

G_{IC} **[N/mm]** [14]	G_{IIC} **[N/mm]** [15]	σ_I^{max} **[MPa]** [14]	σ_{II}^{max} **[MPa]** [14]	α [14]
0.2	0.8	60	90	1.0

Table 1. Cohesive zone interface elements properties of IM7/8552

E_{11}**[GPa]** [14]	$E_{22}=E_{33}$**[GPa]** [14]	$G_{12}=G_{13}$**[GPa]** [14]	G_{23}**[GPa]** [14]	$\alpha_{22}=\alpha_{33}$**[°C^{-1}]** [14]	α_{11}**[°C^{-1}]** [14]
161	11.4	0.517	0.398	3×10^{-5}	0.0
σ_{11t}^{max} **[MPa]** [16]	σ_{11c}^{max} **[MPa]** [16]	σ_{22t}^{max} **[MPa]** [16]	σ_{22c}^{max} **[MPa]** [17]	τ_{12}^{max} **[MPa]** [16]	$\upsilon_{12}=\upsilon_{13}$ [14]
2724	1690	111	255	120	0.320

Table 2. Lamina properties of IM7/8552

The mixed-mode failure criteria of the cohesive zone interface elements are shown in Figure 2.

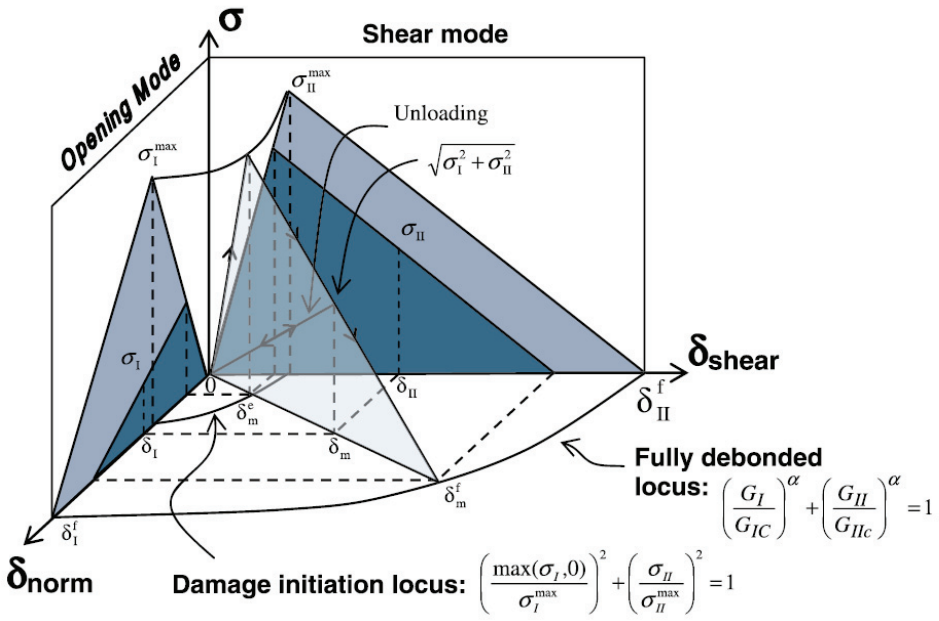

Figure 2. Mixed-mode traction displacement relationship for interface elements[18]

Splitting elements were pre-installed along multiple paths within all plies and delamination elements were pre-installed between all plies with different fibre orientations as shown in Figure 3. Four splitting paths were pre-installed along the fibre direction in each 20° ply, and one splitting path was pre-installed along the fibre direction in each -20° ply. Splits of different orientations are potentially able to join up at 1/8, 1/4, 3/8, 1/2 of the specimen width. This allows the FE code to predict the weakest failure propagation path and also to simulate in a simplified way the interaction between randomly distributed splits and delaminations in the real situation.

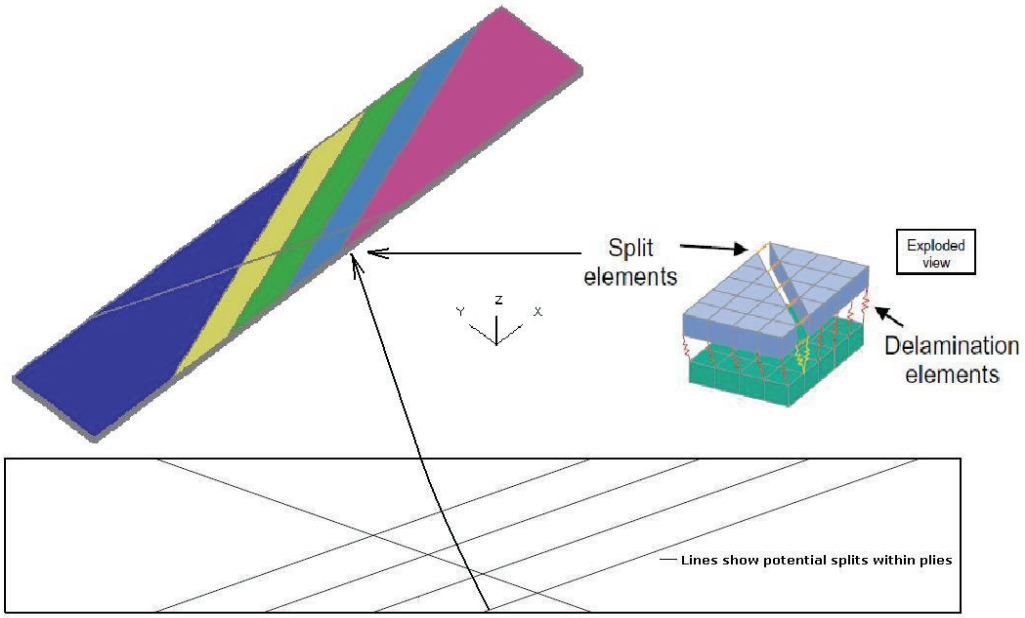

Figure 3. Potential splitting locations

4 Results analysis

4.1 Test results

From the load-displacement curves, it was seen that at first tensile loads increased with displacements linearly. Then, some small load drops happened, but generally the loads kept on rising. Finally, catastrophic failure occurred with a huge load drop to zero. The highest load level before the final load drop was regarded as the failure load from which the average failure stress was calculated based on the measured widths and thicknesses. Test results in Table 3 show a drop in failure stress from the laminates with dispersed plies to blocked plies. In Figure 4, interrupted tests of both dispersed ply laminates and blocked ply laminates showed splits and delaminations initiated from the free edges in the surface ply. When such splits and delaminations propagated, they joined up right through the thickness, and the surface ply peeled off. This led to a sudden loss of stiffness, which caused the final failure of the specimens.

	Mean [MPa]	**CV [%]**
Dispersed ply laminates	1227	3.4
Blocked ply laminates	781	0.9

Table 3. Average failure stresses from the test results

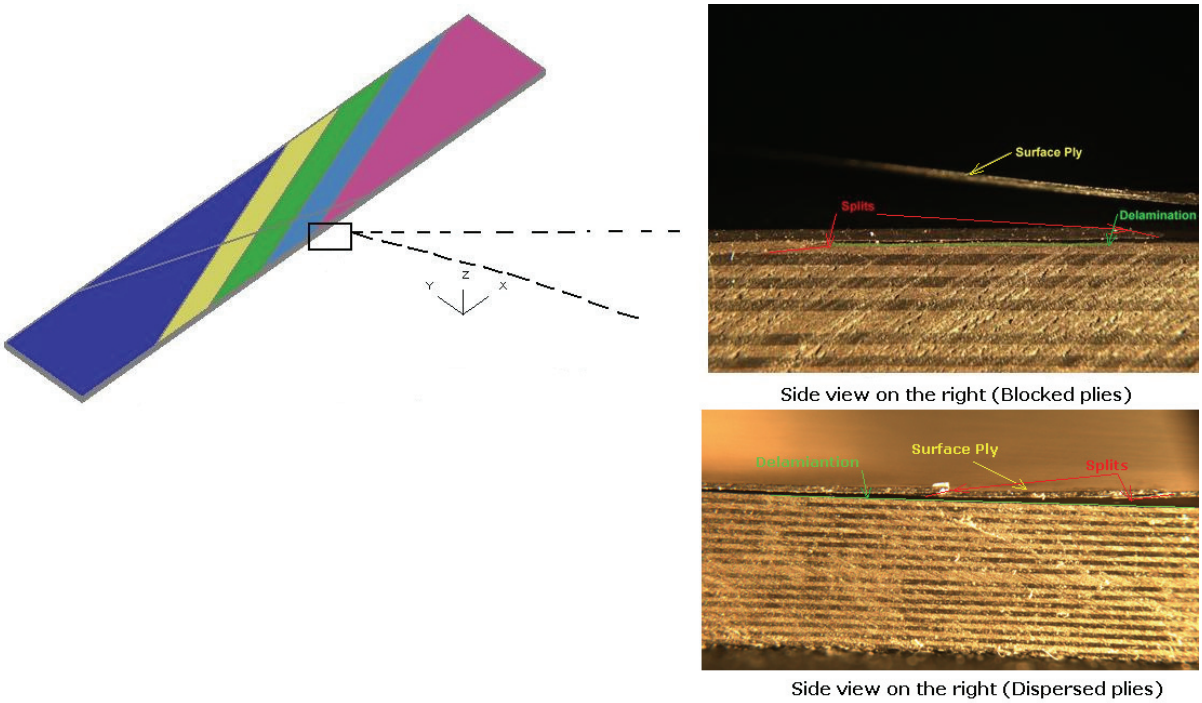

Figure 4. A typical picture showing splits and delaminations in interrupted tests at 90% of the failure load

4.2 FEA results

Figure 5 illustrates tensile stress-strain curves from the FEA. The FEA results agree well with the test results, and show a drop of tensile strength when blocking the plies together.

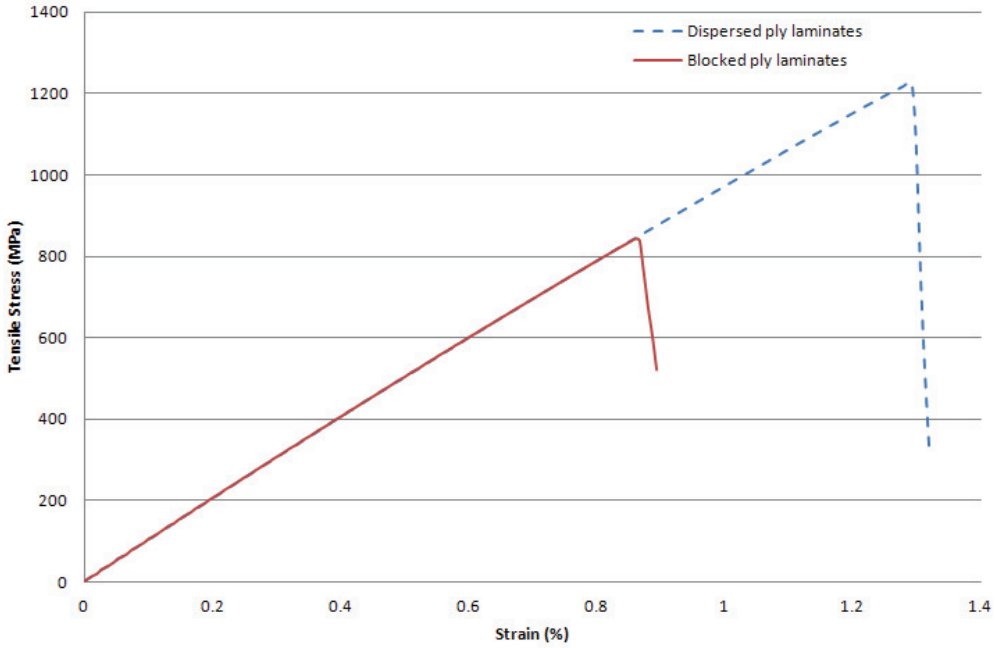

Figure 5. Tensile stress-strain curves from the FEA

Table 4 shows the delamination and splitting pattern of the two lay-ups in the FEA, with the failed elements in red. From the FE results, both edge delaminations and splits initiated from the free edges from the surface ply. Then edge delaminations propagated along with splits and they joined up together, which caused a large amount of surface ply delaminations. This led to a big loss of specimen stiffness. In addition, splits and edge delaminations initiated at lower stress levels for the blocked ply laminates.

	Stress level [MPa]	**Delaminations**		**Splits within plies**
		Surface ply/second ply interface	**Second ply/third ply interface**	**All layers (superimposed)**
Dispersed ply laminates	1094		—	
	1208	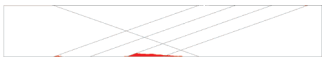		
	1227	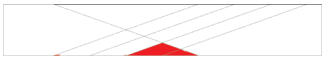	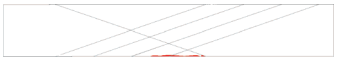	
Blocked ply laminates	818		—	—
	836			
	838	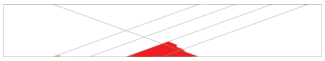	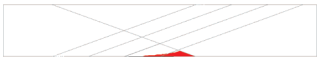	

Table 4. Comparison of delaminations and splits

4.3 Simplified calculation

From the FEA, we knew the surface ply delaminations were mode II dominated, so the critical strain energy release rate used here was mode II. Applying a simplified calculation based on O'Brien's approach[13], the mode II strain energy release rate for full delamination of one ply can be evaluated and equated to the fracture energy. Considering uniform in-plane tensile response and neglecting coupling terms, this gives:

$$G_{\mathrm{IIC}} = \frac{{\sigma_{\mathrm{C}}}^2 t}{2m}\left(\frac{tE_{\mathrm{lam}} - t_{\mathrm{ld}}E_{\mathrm{ld}}}{t_{\mathrm{ld}}E_{\mathrm{lam}}E_{\mathrm{ld}}}\right) \tag{1}$$

where G_{IIC}=0.8 N/mm[15], E_{lam}=104.7 GPa, E_{ld}=104.5 GPa from the CLT calculations, t=4 mm, m is the number of delamination interfaces, and for this surface ply delamination m=1, σ_{C} is the far field stress level. From Equation 1, this gives:

$$\sigma_{\mathrm{C}} = \sqrt{\frac{2mG_{\mathrm{IIC}}t_{\mathrm{ld}}E_{\mathrm{lam}}E_{\mathrm{ld}}}{t(tE_{\mathrm{lam}} - t_{\mathrm{ld}}E_{\mathrm{ld}})}} \tag{2}$$

For the dispersed ply laminates (t_{ld}=3.875 mm), σ_{C} =1139 MPa, and for the blocked ply laminates (t_{ld}=3.75 mm), σ_{C} =792 MPa.

From the experimental and numerical results, final failure happened very soon after edge delamination initiation. So the far field stress for edge delamination initiation can approximately be used as the average failure stress of the specimens. Therefore, the expected failure stress of the dispersed ply laminates is 1139 MPa, and 792 MPa for the blocked ply laminates according to the simplified calculation.

4.4 Results comparison

Results from the tests, FEA, simplified energy based calculations and calculations based on CLT with different stress failure criteria were compared in Table 5. A good correlation between the test and the FEA results was found. The simplified calculation also managed to predict delamination initiation. However, failure theories based on CLT failed to distinguish the two laminate lay-ups. The failure criteria based on CLT are listed from Equation 3 to Equation 5.

	Test	**FEA**	**Simplified calculation**	**Failure theories based on CLT**		
				Max stress	**Tsai-Hill**	**Tsai-Wu**
Dispersed ply laminates	1227	1227	1139	1630	1210	1254
Blocked ply laminates	781	838	792	1630	1210	1254

Table 5. Comparison of average tensile failure stresses from different methods [MPa]

Max stress:
$$\max\left(\left|\frac{\sigma_{11}}{\sigma_{11}^{\max}}\right|, \left|\frac{\sigma_{22}}{\sigma_{22}^{\max}}\right|, \left|\frac{\tau_{12}}{\tau_{12}^{\max}}\right|\right) = 1 \tag{3}$$

Tsai-Hill:
$$\left(\frac{\sigma_{11}}{\sigma_{11}^{\max}}\right)^2 - \frac{\sigma_{11}\sigma_{22}}{\left(\sigma_{11}^{\max}\right)^2} + \left(\frac{\sigma_{22}}{\sigma_{22}^{\max}}\right)^2 + \left(\frac{\tau_{12}}{\tau_{12}^{\max}}\right)^2 = 1 \quad (4)$$

Tsai-Wu:
$$F_1\sigma_{11} + F_2\sigma_{22} + F_{11}\sigma_{11}^2 + 2F_{12}\sigma_{11}\sigma_{22} + F_{22}\sigma_{22}^2 + F_{33}\tau_{12}^2 = 1 \quad (5)$$

where $F_1 = \frac{1}{\left|\sigma_{11t}^{\max}\right|} - \frac{1}{\left|\sigma_{11c}^{\max}\right|}$, $F_2 = \frac{1}{\left|\sigma_{22t}^{\max}\right|} - \frac{1}{\left|\sigma_{22c}^{\max}\right|}$, $F_{11} = \frac{1}{\left|\sigma_{11t}^{\max}\sigma_{11c}^{\max}\right|}$, $F_{22} = \frac{1}{\left|\sigma_{22t}^{\max}\sigma_{22c}^{\max}\right|}$, $F_{33} = \frac{1}{\left(\tau_{12}^{\max}\right)^2}$ and F_{12} can be determined using equibiaxial tests, but for simplification $F_{12} = -\frac{\sqrt{F_{11}F_{22}}}{2}$ was used according to Reference [19].

$\sigma_{11}{}^{\max}$, $\sigma_{22}{}^{\max}$ and $\tau_{12}{}^{\max}$ are the strengths listed in Table 2. Whether they are tension or compression is determined by the CLT calculations. σ_{11}, σ_{22} and τ_{12} are the stresses along the material directions and gained from the CLT calculations. Each of these stresses is identical in the dispersed ply and the blocked ply laminates under the same loads. So the failure theories based on CLT yield the same average failure stresses in the dispersed ply and the blocked ply laminates.

5 Conclusions

Experimental and numerical results showed that the interaction between splits and edge delaminations played a very important role in the failure of angle ply laminates. The joining up of edge delaminations and splits within the surface plies caused a significant loss of stiffness, which led to the final failure of the laminates.

Evidence from both the tests and the FEA showed splits and edge delaminations initiated and propagated at a lower stress level in the blocked ply laminates. This was due to more energy being available in the blocked ply laminates. As a result of edge delaminations, the blocked ply laminates lost stiffness at a lower stress level, which gave rise to a decrease of average tensile strength compared with the laminates with dispersed plies. The FE method in the present study considering the interaction between splits and edge delaminations was very successful in simulating the failure mechanism of both angle ply laminates. In addition, the simplified energy based method used in the present study also predicted the stress for the angle ply edge delamination initiation. By comparison, the results calculated by the failure theories based on CLT were not satisfactory.

Reducing ply thickness can suppress angle ply edge delaminations and increase the strength of angle ply laminates. Thin-ply laminates which have 0.03mm-thick plies are being studied.

References

[1] O'Brien T.K. Characterization of delamination onset and growth in a composite laminate. *Damage in Composite Materials, ASTM STP 775,* pp. 140-167 (1982).
[2] Johnson P., Chang F.K. Characterization of matrix crack-induced laminate failure - Part I: Experiments. *Journal of Composite Materials*, **35**, pp. 2009-2035 (2001).
[3] O'Brien T.K., Hooper S.J. Local Delamination in laminates with angle ply matrix cracks, Part I: Tension tests and stress analysis. *Composite Materials: Fatigue and Fracture, ASTM STP 1156*, **4**, pp. 491-506 (1993).
[4] O'Brien T.K., Hooper S.J. *Local delamination in laminates with angle ply matrix cracks, Part II: Delamination fracture analysis and fatigue characterization* in "*4th ASTM Conference on Composite Materials*", Indiana, USA, (1991).
[5] Yang H.T.Y., He C.C. 3-dimensional finite-elements analysis of free-edge stresses and delamination of composite laminates. *Journal of Composite Materials*, **28**, pp. 1394-1412 (1994).
[6] Lavoie J.A., Morton J. Scaling of first-ply failure and strength in [+theta(n)/-theta(n)/90(2n)](s) laminates: Experiments and predictions. *Journal of Composite Technology & Research,* **22** pp. 153-160 (2000).
[7] Johnson P., Chang F.K. Characterization of matrix crack-induced laminate failure - Part II: Analysis and verifications. *Journal of Composite Materials*, **35**, pp. 2037-2074 (2001).
[8] Kashtalyan M., Soutis C. Strain energy release rate for off-axis ply cracking in laminated composites. *International Journal of Fracture,* **112,** pp. 3-8 (2001).
[9] Kashtalyan M., Soutis C. Analysis of local delaminations in composite laminates with angle-ply matrix cracks. *International Journal of Solids and Structures*, **39**, pp. 1515-1537 (2002).
[10] Kashtalyan M., Soutis C. Stiffness and fracture analysis of laminated composites with off-axis ply matrix cracking. *Composites Part A: Applied Science and Manufacturing,* **38**, 1262-1269 (2007).
[11] Kobayashi S., Tanaka A., Wakayama S. *Characterization of off-axis ply cracking behavior in CFRP laminates* in "Proceeding of *4th Joint Canada/Japan Workshop on Composites* ", Vancouver, Canada, (2002).
[12] Kellas S., Morton J. Strength scaling in fiber composites. *AIAA Journal,* **30** pp. 1074-1080 (1992).
[13] O'Brien T.K. Analysis of local delaminations and their influence on composite laminate behavior. *Delamination and Debonding of Materials ASTM STP 876*, pp. 282-297 (1985).
[14] Hallett S.R., Green B.G., Jiang W-G., Wisnom M.R. An experimental and numerical investigation into the damage mechanisms in notched composites. *Composites Part A: Applied Science and Manufacturing,* **40** pp. 613-624 (2009).
[15] O'Brien T.K., Johnston W.M., Toland G.J. Mode II interlaminar fracture toughness and fatigue characterization of a graphite epoxy composite material. *NASA/TM–2010-216838* (2010).
[16] Hexcel Corporation. HexPly® IM7/8552 Product Data, (2008), from http://www.hexcel.com/Resources/DataSheets/Prepreg-Data-Sheets/8552_eu.pdf
[17] Koerber H., Xavier J., Camanho P.P. High strain rate characterization of unidirectional carbon-epoxy IM7-8552 in transverse compression and in-plane shear using digital image correlation. *Mechanics of Materials,* **42** pp. 1004-1019 (2010).
[18] Jiang W-G., Hallett S.R., Green B.G., Wisnom M.R. A concise interface constitutive law for analysis of delamination and splitting in composite materials and its application to scaled notched tensile specimens. *International Journal for Numerical Methods in Engineering*, **69** pp. 1982-1995 (2007).
[19] Tsai S.W., Hahn H.T. *Introduction to composite materials.* Technomic Publishing Co., Lancaster, USA, (1980).